INT. J. NUM. METH. HEAT FLUID FLOW, VOL. 6, NO. 6, 3–23 (1996)

# STEADY-STATE SOLUTIONS OF BUOYANCY-ASSISTED INTERNAL FLOWS USING A FAST FALSE IMPLICIT TRANSIENT SCHEME (FITS)

M.M. EL-REFAEE†, M.M. ELSAYED†, N.M. AL-NAJEM AND I.E. MEGAHID‡

†*Mechanical and Industrial Engineering Department, Kuwait University, Kuwait*
‡*Mechanical Engineering Department, King Abdulaziz University, Jeddah, Saudi Arabia*

## ABSTRACT

A fast false implicit transient scheme FITS is developed to predict the two-dimensional steady-state solutions of buoyancy-assisted laminar internal flows. This new scheme uses the control volume based on power law technique in conjugation with the alternating direction implicit (ADI) and the successive grid refinement (SGR) procedures to solve the transient vorticity and energy transport equations. The ADI procedure allows the power law, which gives an excellent approximation to the exact 1-D solution, to be applied locally in one-dimensional sense for each sweep in the co-ordinates' directions. This in turn increased the solution accuracy and hence permits the use of a larger time increment. As a result a remarkable increase in the convergence rate to steady-state is achieved. The final solution is obtained by successively refining the grid as the solution advances in time. The efficiency of FITS is verified by comparing the present predictions with three steady-state benchmark solutions: natural convection of a heat generating fluid in a rectangular enclosure, natural convection inside a cavity with two isothermal walls, and a vertical buoyancy-assisted laminar backward-facing step flow.

KEY WORDS Buoyancy-assisted laminar internal flows False implicit transient scheme Steady-state solutions

## NOMENCLATURE

$a_{i,j}$ = coefficient of finite difference equation at point $(i,j)$ in a grid
$A$ = function of power law
$b$ = right hand side of finite difference equation
$c_p$ = specific heat constant pressure
$Gr$ = Grashof number
$g$ = gravitational acceleration
$H$ = characteristic length
$k$ = thermal conductivity of the fluid in the cavity
$Pe$ = cell Peclet number, = $U\Delta X/\Gamma$ or $V\Delta Y/\Gamma$
$Pr$ = Prandtl number of the fluid in the cavity
$q'''$ = rate of volumetric heat generation of the fluid in the cavity
$Re$ = Reynolds number
$S_\phi$ = source term, see equation (13)
$T$ = temperature
$T_0$ = reference temperature
$t$ = time
$U$ = dimensionless velocity component in horizontal direction
$u_{ref}$ = reference velocity
$V$ = dimensionless velocity component in vertical direction
$v$ = velocity component in vertical direction
$X$ = dimensionless horizontal distance
$x$ = horizontal distance
$Y$ = dimensionless vertical distance
$y$ = vertical distance
$\beta$ = coefficient of thermal expansion
$\Gamma_\phi$ = diffusion coefficient in equation (13)
$\Delta T_{ref}$ = reference temperature difference
$\theta$ = dimensionless distance
$\upsilon$ = kinematic diffusivity
$\rho_0$ = density at reference temperature T0
$\tau$ = dimensionless time
$\phi$ = general dependant variable, see equation 13
$\Psi$ = dimensionless stream function
$\psi$ = stream function
$\Omega$ = dimensionless velocity
$\omega$ = vorticity

*Subscripts*
$i$ = $X$ location of a grid point
$j$ = $Y$ location of a grid point

*Superscripts*
$k$ = iteration number for solving $\Omega$ and $\theta$ equations
$m$ = iteration number for solving $\Psi$ equations
$n$ = time level

0961–5539

*Revised January 1996*

## INTRODUCTION

A large share of thermal applications of buoyancy-assisted internal flows require steady-state solutions. The mathematical formulations that are currently used to model the steady two-dimensional buoyancy-driven internal flows can be categorized as:

(1) the steady-state primitive variables formulation;
(2) the transient-primitive variables formulation;
(3) the steady-state derived variables formulation (vorticity-temperature-stream function) and
(4) the transient-derived variables formulation.

In the steady-state formulation cases, a good initial guess for the steady-state solution is required to assure fast convergence. This disadvantage generally leads to a time-consuming trial and error procedure. The difficulty becomes even worse when a fine grid is selected to improve the accuracy of the solution. For these reasons, the transient mathematical models are commonly used to obtain steady-state solutions.

Transient formulations are not, however, guaranteed to give converged steady-state solutions. Flow non-linearities usually impose a stability restriction on the time step even for implicit solutions. The question is: is it possible to devise a fast numerical scheme that uses large time increment to advance the pseudo-transient solution to steady-state? Little, however, has been given in the literature in this direction[1,2].

In the present work the common 2-D transient-derived variables formulation (vorticity-temperature-stream function) is used to model the buoyancy-assisted internal flows. The control volume based power law discretization scheme is implemented in the ADI spatial and the successive grid refinement temporal environments to predict fast steady-state solutions. The developed scheme is named the False Implicit Transient Scheme (FITS). In the next sections, the details of FITS are outlined. Quantitative and qualitative comparisons with benchmark solutions are presented to verify the efficiency and efficacy of the scheme to many buoyancy-assisted laminar internal flow problems.

## FORMULATION

The governing conservation equations for two dimensional flow are given as follows

$$\frac{\partial u}{\partial x} + \frac{\partial v}{\partial y} = 0 \tag{1}$$

$$\frac{\partial u}{\partial t} + u\frac{\partial u}{\partial x} + v\frac{\partial u}{\partial y} = \frac{-1}{\rho_0}\frac{\partial p}{\partial x} + \upsilon\left(\frac{\partial^2 u}{\partial x^2} + \frac{\partial^2 u}{\partial y^2}\right) \tag{2}$$

$$\frac{\partial u}{\partial t} + u\frac{\partial v}{\partial x} + v\frac{\partial v}{\partial y} = \frac{-1}{\rho_0} + \frac{\partial p}{\partial y} + g\beta(T - T_0) + \upsilon\left(\frac{\partial^2 v}{\partial x^2} + \frac{\partial^2 v}{\partial y^2}\right) \tag{3}$$

$$\frac{\partial T}{\partial t} + u\frac{\partial T}{\partial x} + v\frac{\partial T}{\partial y} = \frac{k}{\rho_0 c_p}\left(\frac{\partial^2 T}{\partial x^2} + \frac{\partial^2 T}{\partial y^2}\right) + \frac{q'''}{p_0 c_p} \tag{4}$$

where the Cartesian co-ordinates $x$ and $y$ represent horizontal and vertical distances, $u$ and $v$ are the velocity components in these directions, respectively, $p$ is the pressure, $T$ is the temperature and $t$ is the time. The properties $\rho$, $v$, $k$, $c_p$ and $\beta$ are assumed constant except for the variation of density which is considered only in the buoyancy force through using the expression of Boussinesq. The

above governing equations also assume a volumetric local heat source/sink at a rate of $q'''$ $(x,y,t)$ per unit volume of the fluid.

Using the stream function $\psi$ and the vorticity $\omega$, equations (1) to (4) are reduced to the following

$$\omega = -\left(\frac{\partial^2\psi}{\partial x^2} + \frac{\partial^2\psi}{\partial y^2}\right) \tag{5}$$

$$\frac{\partial\omega}{\partial t} + u\frac{\partial\omega}{\partial t} + v\frac{\partial\omega}{\partial y} = g\beta\frac{\partial T}{\partial x} + \upsilon\left(\frac{\partial^2\omega}{\partial x^2} + \frac{\partial^2\omega}{\partial y^2}\right) \tag{6}$$

$$\frac{\partial T}{\partial t} + u\frac{\partial T}{\partial x} + v\frac{\partial T}{\partial y^2} = \frac{k}{\rho_0 c_p}\left(\frac{\partial^2 T}{\partial x^2} + \frac{\partial^2 T}{\partial y^2}\right) + \frac{q'''}{\rho_0 c_p}. \tag{7}$$

Introducing the following dimensionless quantities

$$\left.\begin{aligned} X &= \frac{x}{H} & Y &= \frac{y}{H} \\ U &= \frac{u}{u_{ref}} & V &= \frac{u}{u_{ref}} \\ q &= \frac{T - T_{ref}}{DT_{ref}} & \tau &= \frac{tu_{ref}}{H} \\ Y &= \frac{y}{u_{ref}} & W &= \frac{wH}{u_{ref}} \end{aligned}\right\} \tag{8}$$

the dimensionless governing equations become:

$$\Omega = -\left(\frac{\partial^2\Psi}{\partial X^2} + \frac{\partial^2\Psi}{\partial Y^2}\right) \tag{9}$$

$$\frac{\partial\Omega}{\partial\tau} + \mathbf{U}\frac{\partial\Omega}{\partial\mathbf{Y}} + \mathbf{V}\frac{\partial\Omega}{\partial\mathbf{Y}} = \frac{Gr}{Re^2}\frac{\partial\theta}{\partial\mathbf{X}} + \frac{1}{Re}\left(\frac{\partial^2\Omega}{\partial\mathbf{X}^2} + \frac{\partial^2\Omega}{\partial\mathbf{Y}^2}\right) \tag{10}$$

$$\frac{\partial\theta}{\partial\tau} + \mathbf{U}\frac{\partial\theta}{\partial\mathbf{X}} + \mathbf{V}\frac{\partial\theta}{\partial\mathbf{Y}} = \frac{1}{RePr}\left(\frac{\partial^2\theta}{\partial\mathbf{X}^2} + \frac{\partial^2\theta}{\partial\mathbf{Y}^2}\right) + \frac{\mathbf{q'''H}}{\rho_0\mathbf{c}_p\Delta\mathbf{T}_{ref}\,\mathbf{u}_{ref}} \tag{11}$$

$$Re = \frac{u_{ref}H}{\upsilon},\ Pr = \frac{\rho_0\upsilon c_p}{k},\ Gr = \frac{g\beta\Delta T_{ref}H^3}{\upsilon^2}. \tag{12}$$

The vorticity and temperature governing equations may now be rewritten in the following general form

$$\frac{\partial\phi}{\partial\tau} + U\frac{\partial\phi}{\partial X} + V\frac{\partial\phi}{\partial Y} = \Gamma_\phi\left(\frac{\partial^2\phi}{\partial X^2} + V\frac{\partial^2\phi}{\partial Y^2}\right) + S_\phi \tag{13}$$

where $\phi$ stands for $\Omega$ or $\theta$ and the expressions for $\Gamma_\phi$ and $S_\phi$ are listed in Table I. For example, these parameters for a step flow are given as follows

$$\left.\begin{aligned} \Gamma_\Omega &= \frac{1}{Re} & S_\Omega &= \frac{Gr}{Re^2}\frac{\partial\theta}{\partial X} \\ \Gamma_\theta &= \frac{1}{RePr} & S_\theta &= \frac{q'''H}{\rho_0 c_p\Delta T_{ref}\,u_{ref}}. \end{aligned}\right\} \tag{14}$$

## THE DISCRETIZATION EQUATIONS

The previous governing equations are uniformly discretized using the control volume approach. The power law is employed in discretizing the convection and diffusion terms as described by Patankar[3]. To accelerate the convergence an alternating direction implicit (ADI) scheme is employed[4]. In fact, the implementation of the ADI procedure enhances the accuracy of the solution since it allows the power law to be applied locally in a one-dimensional sense for each sweep in the co-ordinate directions. The resultant discretized form of equations (13) in the $x$ and $y$ directions are given respectively as follows:

$$-a_{i-1,j}^{n+\frac{1}{2}}\,\phi_{i-1,j}^{n+\frac{1}{2}} + a_{i,j}^{n+\frac{1}{2}}\,\phi_{i,j}^{n+\frac{1}{2}} - a_{i+1,j}^{n+\frac{1}{2}}\,\phi_{i+1,j}^{n+\frac{1}{2}} = b^{n} \tag{15}$$

$$-a_{i,j-1}^{n+1}\,\phi_{i,j-1}^{n+1} + a_{i,j}^{n+1}\,\phi_{i,j}^{n+1} - a_{i,j+1}^{n+1}\,\phi_{i,j+1}^{n+1} = b^{n+\frac{1}{2}} \tag{16}$$

where the subscripts $i$ and $j$ refer respectively to the $X$ and $Y$ locations of the grid point and the superscripts $n$, $n+\frac{1}{2}$, $n+1$ indicate respectively, old time, advancing a half time step and advancing a full time step. The coefficients of equations (15) and (16) are expressed as follows

$$\left.\begin{aligned}
a_{i-1,j}^{n+\frac{1}{2}} &= \frac{\Delta\tau\Gamma_{\phi}}{\Delta X^{2}}\,\mathrm{A}\left(\left|\mathrm{P}_{i-\frac{1}{2},j}^{n+\frac{1}{2}}\right|\right) + \frac{\Delta\tau}{\Delta X}\left[\left[\mathrm{U}_{i-\frac{1}{2},j}^{n+\frac{1}{2}}, 0\right]\right]\\
a_{i+1,j}^{n+\frac{1}{2}} &= \frac{\Delta\tau\Gamma_{\phi}}{\Delta X^{2}}\,\mathrm{A}\left(\left|\mathrm{P}_{i+\frac{1}{2},j}^{n+\frac{1}{2}}\right|\right) + \frac{\Delta\tau}{\Delta X}\left[\left[-\mathrm{U}_{i+\frac{1}{2},j}^{n+\frac{1}{2}}, 0\right]\right]\\
a_{i,j}^{n+\frac{1}{2}} &= 2 + a_{i-1,j}^{n+\frac{1}{2}} + a_{i+1,j}^{n+\frac{1}{2}}\\
b^{n} &= 2\phi_{i,j}^{n} + \frac{\Delta\tau\Gamma_{\phi}}{\Delta Y^{2}}\left\{\mathrm{A}\left(\left|\mathrm{P}_{i,j+\frac{1}{2}}^{n}\right|\right)\cdot\left(\phi_{i,j+1}^{n} - \phi_{i,j}^{n}\right) + \mathrm{A}\left(\left|\mathrm{P}_{i,j-\frac{1}{2}}^{n}\right|\right)\cdot\left(\phi_{i,j-1}^{n} - \phi_{i,j}^{n}\right)\right\}\\
&\quad + \frac{\Delta\tau}{\Delta Y}\left\{\left[\left[-\mathrm{V}_{i,j+\frac{1}{2}}^{n}, 0\right]\right]\left(\phi_{i,j+1}^{n} - \phi_{i,j}^{n}\right) + \left[\left[-\mathrm{V}_{i,j-\frac{1}{2}}^{n}, 0\right]\right]\left(\phi_{i,j-1}^{n} - \phi_{i,j}^{n}\right)\right\} + \Delta\tau.S_{\phi}^{n}
\end{aligned}\right\} \tag{17a}$$

$$\left.\begin{aligned}
a_{i,j-1}^{n+\frac{1}{2}} &= \frac{\Delta\tau\Gamma_{\phi}}{\Delta Y^{2}}\,\mathrm{A}\left(\left|\mathrm{P}_{ij,-\frac{1}{2}}^{n+1}\right|\right) + \frac{\Delta\tau}{\Delta Y}\left[\left[\mathrm{V}_{i,j-\frac{1}{2}}^{n+1}, 0\right]\right]\\
a_{i,j+1}^{n+1} &= \frac{\Delta\tau\Gamma_{\phi}}{\Delta Y^{2}}\,\mathrm{A}\left(\left|\mathrm{P}_{i,j+\frac{1}{2}}^{n+1}\right|\right) + \frac{\Delta\tau}{\Delta Y}\left[\left[-\mathrm{V}_{i,j+\frac{1}{2}}^{n+1}, 0\right]\right]\\
a_{i,j}^{n+1} &= 2 + a_{i,j-1}^{n+1} + a_{i,j+1}^{n+1}\\
b^{n+\frac{1}{2}} &= 2\phi_{i,j}^{n+\frac{1}{2}} + \frac{\Delta\tau\Gamma_{\phi}}{\Delta X^{2}}\left\{\mathrm{A}\left(\left|\mathrm{P}_{i+\frac{1}{2},j}^{n+\frac{1}{2}}\right|\right)\cdot\left(\phi_{i+1,j}^{n+\frac{1}{2}} - \phi_{i,j}^{n+\frac{1}{2}}\right) + \mathrm{A}\left(\left|\mathrm{P}_{i-\frac{1}{2},j}^{n+\frac{1}{2}}\right|\right)\cdot\left(\phi_{i-1,j}^{n+\frac{1}{2}} - \phi_{i,j}^{n+\frac{1}{2}}\right)\right\}\\
&\quad + \frac{\Delta\tau}{\Delta X}\left\{\left[\left[-\mathrm{U}_{i+\frac{1}{2},j}^{n+\frac{1}{2}}, 0\right]\right]\left(\phi_{i+1,j}^{n+\frac{1}{2}} - \phi_{i,j}^{n+\frac{1}{2}}\right) + \left[\left[\mathrm{U}_{i-\frac{1}{2},j}^{n+\frac{1}{2}}, 0\right]\right]\left(\phi_{i-1,j}^{n+\frac{1}{2}} - \phi_{i,j}^{n+\frac{1}{2}}\right)\right\} + \Delta\tau.S_{\phi}^{n+\frac{1}{2}}
\end{aligned}\right\} \tag{17b}$$

where

$$\left.\begin{aligned} U_{i\pm\frac{1}{2},j} &= \frac{1}{2}\left(U_{i,j} + U_{i\pm1,j}\right) \\ V_{i,j\pm\frac{1}{2}} &= \frac{1}{2}\left(V_{i,j} + V_{i\pm1,j}\right) \\ U_{i,j}^{n+\frac{1}{2}} &= \frac{1}{2}\left(U_{i,j}^{n} + U_{i,j}^{n+1}\right) \end{aligned}\right\} \tag{18}$$

$$\left.\begin{aligned} P_{i\pm\frac{1}{2},j} &= \frac{\Delta X}{\Gamma_\phi}\frac{1}{2}\left(U_{i,j} + U_{i\pm1,j}\right) \\ P_{i,j\pm\frac{1}{2}} &= \frac{\Delta Y}{\Gamma_\phi}\frac{1}{2}\left(V_{i,j} + V_{i,j\pm1}\right). \end{aligned}\right\} \tag{19}$$

The function $A(|P|)$ in equations (16) and (17) is given by the following expression[3]

$$A(|P|) = \left[\left[0, (1 - 0.1|P|)^5\right]\right] \tag{20}$$

where the operator $[[a,b]]$ indicates the greater of $a$ and $b$.

To complete the discretization process, the flow kinematics equation, equation (9), is discretized using central difference. The final form of the equation becomes

$$\Psi_{i,j}^{n+1} = \frac{\Delta Y^2}{2(\Delta X^2 + \Delta Y^2)}\left(\Psi_{i+1,j}^{n+1} + \Psi_{i-1,j}^{n+1}\right) + \frac{\Delta Y^2}{2(\Delta X^2 + \Delta Y^2)}\left(\Psi_{i,j+1}^{n+1} + \Psi_{i,j-1}^{n+1}\right) + \frac{\Delta X^2 \Delta Y^2}{2(\Delta X^2 + \Delta Y^2)}\Omega_{i,j}^{n+1} \tag{21}$$

Once $\Psi_{i,j}^{n+1}$ is calculated $U_{i,j}^{n+1}$ and $V_{i,j}^{n+1}$ are determined as follows:

$$\left.\begin{aligned} U_{i,j}^{n+1} &= \frac{1}{2\Delta Y}\left(\Psi_{i,j+1}^{n+1} + \Psi_{i,j-1}^{n+1}\right) \\ V_{i,j}^{n+1} &= \frac{1}{2\Delta X}\left(\Psi_{i-1,j}^{n+1} + \Psi_{i+1,j}^{n+1}\right). \end{aligned}\right\} \tag{22}$$

## FITS ALGORITHM

In the previous section the discretization equations are given for the field variables $\Omega^{n+1}$, $\theta^{n+1}$ and $\Psi^{n+1}$. To solve the equations of $\Omega$ and $\theta$, one must know in advance the values of $U_{n+1}$ and $V^{n+1}$. Since they are not known, an iteration procedure will be followed. For each iteration, the linearized equations for $\theta$ and $\Omega$ (equations 15) and (16)) are sequentially solved using the Thomas line Tri-Diagonal Matrix Algorithm[5]. Successive over-relaxation procedure is then used to iterate for the stream function $\Psi$ resulting in the following expression:

$$\left(\Psi_{i,j}^{n+1}\right)^{m+1} = (1-\lambda)\left(\Psi_{i,j}^{n+1}\right)^{m} + \frac{\lambda}{2(\Delta X^2 + \Delta Y^2)}\left[\Delta X^2\left(\Psi_{i,j+1}^{n+1} + \Psi_{i,j-1}^{n+1}\right)^{m} + \Delta Y^2\left(\Psi_{i+1,j}^{n+1} + \Psi_{i-1,j}^{n+1}\right)^{m} + \Delta X^2 \Delta Y^2\left(\Omega_{i,j}^{n+1}\right)^{k}\right] \tag{23}$$

where $\lambda$ is the over-relaxation factor which is given as follows:

$$\lambda = \frac{8 - 4\sqrt{4 - \alpha^2}}{\alpha} \tag{24}$$

with

$$\alpha = \cos\left(\frac{\pi}{M}\right) + \cos\left(\frac{\pi}{N}\right) \tag{25}$$

and $M$ and $N$ are the number of grid points in the $X$ and $Y$ directions, respectively.

The transient solution is advanced with a time step $\Delta\tau$, until steady-state solution is obtained. Since accuracy of the transient solution at any time level is not important, we may sacrifice the accuracy with the computational efficiency. This may be obtained by using fewer iterations for $\Omega$, $\theta$, $\Psi$.

Basically, implicit schemes are unconditionally stable for linear problems. Consequently, no restrictions on the time step nor are the Courant and cell Reynolds numbers imposed. For non-linear problems, however, the time step is restricted by a weak stability condition[6]. Such non-linear problems are commonly solved by a quasi-linearization approach where the non-linear coefficients are calculated at the previous time level[6-8].

The proposed scheme FITS considerably relieve the above weak stability condition, allowing a larger time step to be used for the solution of the present non-linear vorticity and energy transport equations. This major advantage may be attributed to the fact that FITS continuously fits the I-D exact solution for each sweep of the ADI procedure (see the section on the discretization equations).

The application of the successive grid-refinement procedure is found to be very effective in increasing the computational speed. Steady-state solutions obtained from coarser grids are linearly interpolated and successively used as an initial distribution in the next finer grid.

The fast False Implicit Transient Scheme (FITS) may be outlined as follows

(1) Select a coarse grid. A grid 11 × 11 is a good start in many cases.
(2) Use trial and error procedure to select the corresponding largest possible time step.
(3) Assume a initial solutions for $U_n$, $V_n$, $\theta n$, $\Omega_n$ or get these values at an earlier time level.
(4) As a first trial assign the values of $U_n$ and $V_n$ to $U^{n+1}$ and $V^{n+1}$.
(5) Use $U^{n+1}$ and $V^{n+1}$ to calculate $\theta^{n+1}$ using equations (15) and (16) with $\phi$ to stand for $\theta$.
(6) Use the values of $U^{n+1}$, $V^{n+1}$, and $\theta^{n+1}$ to determine $\Omega^{n+1}$ from equations (15) and (16).
(7) Solve equation 21 to determine $\Psi^{n+1}$.
(8) Determine new values of $U^{n+1}$ and $V^{n+1}$ from the values of $\Psi^{n+1}$ using central difference given by equation (22).
(9) Use the new values of $U^{n+1}$ and $V^{n+1}$ to repeat steps 5 to 8. Check convergence of $\Omega^{n+1}$ and $\theta^{n+1}$ if not converged repeat steps 5 to 8.
(10) Repeat steps 4 to 9 for advancing time levels until steady-state convergence is achieved.
(11) Repeat steps 2 to 10 successively for refined grids.
(12) Check the solution grid-independence by comparing the results obtained from two successive grids and repeat step 11 if necessary.

## NATURAL CONVECTION OF HEAT-GENERATING FLUID IN A RECTANGULAR ENCLOSURE

Thermal convection in a fluid with internal energy sources is of major interest in nuclear reactor safety analysis[9]. Other applications include chemical engineering processes in fluids and microwave heating. In this benchmark problem, the present FITS is used to predict a steady-state solution of a 2-D laminar natural convection inside a square cavity that contains fluid with

homogeneous sources of internal energy and is bounded by four isothermal walls. The reference physical parameters (height, velocity, and temperature difference) together with the coefficients of equation (13) ($\Gamma_\phi$, $S_\phi$) are given in *Table 1*. Churbanov *et al.*[9] showed that a steady-state regime or an oscillating flow regime may be obtained depending on the aspect ratio of the cavity and the value of the Rayleigh number. In the present investigation we consider only the steady-state solution for a square cavity with $Ra = 6.4 \times 10^5$ and $Pr = 7$.

The solution for this flow was initiated by using a coarse grid(11 × 11). The grid was successively refined as the solution advances in time. The time step and the CPU time required to achieve converged solutions are listed in *Table 2* against the grids. The convergence criterion to reach a steady-state solution was the standard relative error based on the maximum-norm ($\lambda$):

$$\lambda = \frac{\left\|\Omega^{n+1} - \Omega^n\right\|_\infty}{\left\|\Omega^{n+1}\right\|_\infty} + \frac{\left\|\theta^{n+1} - \theta^n\right\|_\infty}{\left\|\theta^{n+1}\right\|_\infty} \leq 10^{-6} \tag{26}$$

where the operator $\|\eta\|_\infty$ indicates the maximum absolute value of the variable over all the grid points in the computational domain.

Grid independence tests were carried out with five uniform grids of 11 × 11, 21 × 21, 31 × 31, 41 × 41 and 81 × 81. It is evident in *Figure* 1 that the temperature distribution of the 41 × 41 grid

*Table 1* Definition of the reference height, velocity and temperature difference in the present problems and the related coefficients to the governing differential equations

| Parameter | Cavity with heat generation | Thermal cavity | Step flow |
|---|---|---|---|
| $H$ | Height of cavity | $H$ | $s$ |
| $u_{\text{ref}}$ | $\nu/H$ | $\sqrt{g\beta\Delta T_{\text{ref}} H}$ | $\bar{v}$ |
| $\Delta T_{\text{ref}}$ | $q''' H / k$ | $T_H - T_c$ | $T_w - T_o$ |
| $\Gamma_\Omega$ | 1 | $\left(\frac{Ra}{Pr}\right)^{\frac{-1}{2}} = \left(\frac{gbDT_{\text{ref}} H^3}{\nu^2}\right)^{\frac{-1}{2}}$ | $\frac{\upsilon}{\bar{v}s} = \frac{1}{Re_s}$ |
| $S_\Omega$ | $\frac{1}{pr}$ | $\frac{\partial\theta}{\partial X}$ | $\frac{g\beta\Delta T_{\text{ref}} s}{\bar{v}} \frac{\partial\theta}{\partial x} = \frac{Gr_s}{Re_s^2} \frac{\partial\theta}{\partial x}$ |
| $\Gamma_\theta$ | $\frac{1}{pr}$ | $(RaPr)^{\frac{-1}{2}} = \left(\frac{gbDT_{\text{ref}} H^3}{\alpha^2}\right)^{\frac{-1}{2}}$ | $\frac{\alpha}{\bar{v}s} = \frac{1}{Pe_s}$ |
| $S_\theta$ | $\frac{g\beta q''' H^5}{k\upsilon^2} \frac{\partial\theta}{\partial x} = \frac{Ra}{Pr} \frac{\partial\theta}{\partial x}$ | 0 | 0 |

*Table 2* The present CPU time and time step $\Delta\tau$ of the successive grids used for the case of heat generating fluid

| Grid system | 11 × 11 | 21 × 21 | 41 × 41 | 81 × 81 |
|---|---|---|---|---|
| CPU[a] (min) | 0.5 | 1.1 | 4.2 | 8.7 |
| Dt | 0.16 | 0.14 | 0.11 | 0.08 |

Note: [a]VAX 9000/420 Super-mini (scalar mode)

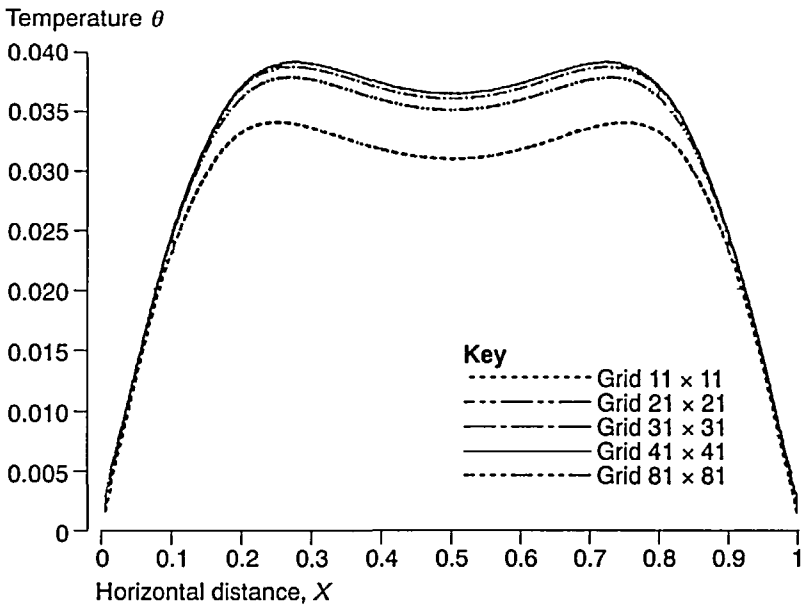


*Figure 1* Temperature distribution at the horizontal mid-plane for the case of a heat-generating fluid in a rectangular cavity

is independent of the grid size. The vertical velocity profiles for different grids were compared in *Figure 2*. As expected, the maximum difference between 11 × 11 and 21 × 21 grids was 16 per cent, whereas the maximum difference between 31 × 31 and 41 × 41 grids was less than 1.5 per

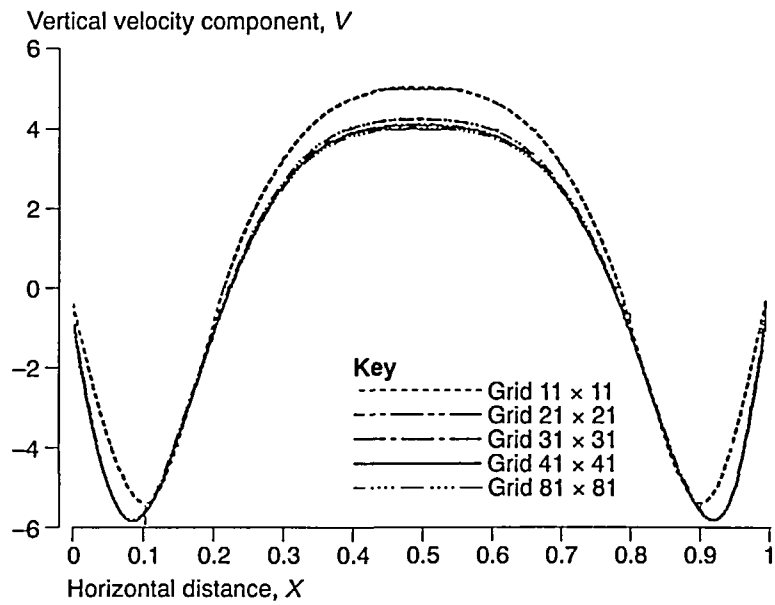


*Figure 2* Vertical velocity profile along the horizontal mid-plane for the case of a heat-generating fluid in a rectangular cavity

cent. It can be concluded from *Figures 1* and *2* that the solutions for the 41 × 41 and 81 × 81 grids are identical for both $\theta$ and $V$.

*Figure 3* depicts a comparison of the present isotherms and streamlines with those given by Churbanov *et al.*[9]. It is evident in the figure that the two sets of contours are in excellent agreement. Moreover, *Table 3* confirms this agreement where the values of $\Psi_{max}$, $\Psi_{min}$, $\theta_{max}$ and their locations are compared.

## NATURAL CONVECTION IN A CAVITY WITH ISOTHERMAL VERTICAL WALLS

Natural convection in enclosures has been the subject of experimental and numerical research over the past two decades due to its importance in applications such as materials processing, solar receivers and concentrators, storage tanks and electronic equipment aircooling. An extensive review of natural convection in enclosure was given by Ostarch[10]. For this reason, the cavity problem has been considered by many investigators as an important benchmark problem for validation and evaluation of numerical schemes.

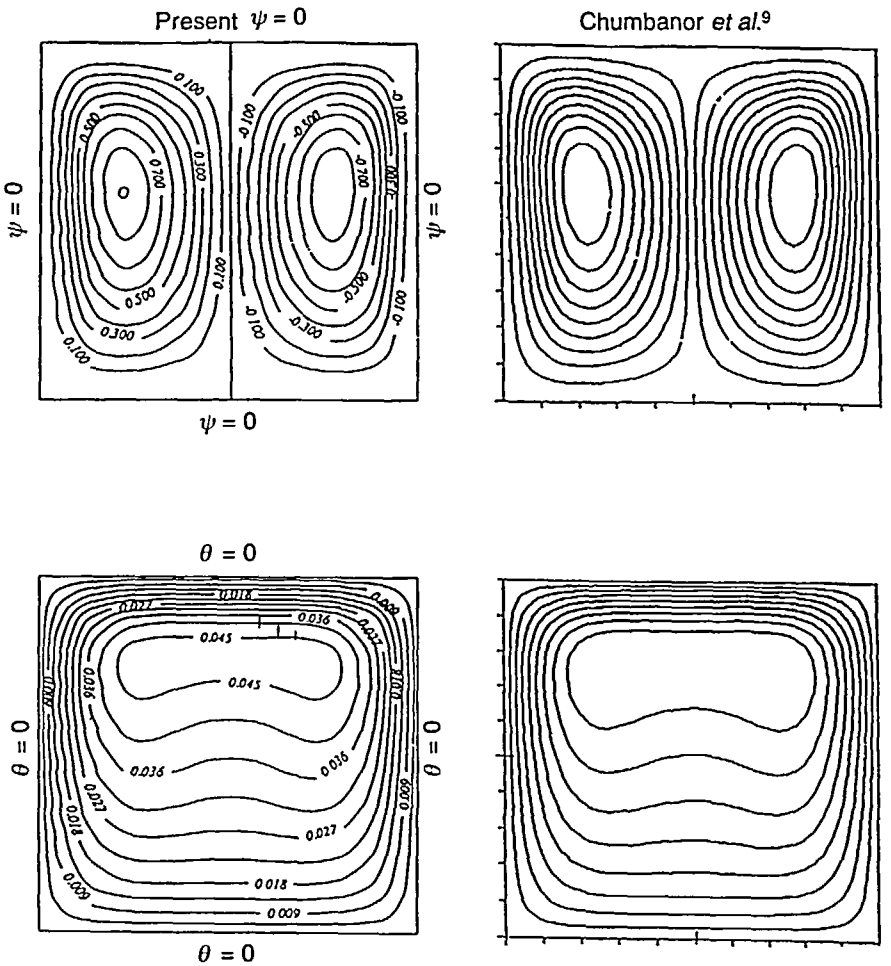


*Figure 3* Streamlines and isotherms in a thermal cavity with a heat-generating fluid at $Ra = 6.4 \times 10^5$

*Table 3* Comparison of the present results for the $\hat{\Psi}_{max}$, $\hat{\Psi}_{min}$, $\theta_{max}$ and their locations with those reported by Churbanov *et al.*[9]

| Parameter | Present | Churbanov *et al.*[9] |
|---|---|---|
| $\hat{\Psi}_{max}[x, y]$ | 0.8806[0.225, 0.575] | 0.8878[0.225, 0.575] |
| $\hat{\Psi}_{min}[x, y]$ | −0.0880[0.775, 0.575] | −0.0878[0.775, 0.575] |
| $\theta_{max}[x, y]$ | 0.0475[0.3, 0.775] [0.7, 0.775] | 0.0477[0.3, 0.760] [0.7, 0.760] |

Note: $\hat{\Psi}$ is defined here with respect to the kinematic viscosity $\upsilon$ ($\hat{Y} = \frac{Y}{u}$)

In the present benchmark problem, we considered 2-D square cavity with two adiabatic horizontal walls (top and bottom) and two isothermal vertical walls (left and right). The left vertical wall is maintained at a hot temperature $T_H$ while the right wall is maintained at a cold temperature $T_c$. *Table 1* describes the reference parameters (height, velocity, and temperature difference) that were used to derive the dimensionless equations as well as the coefficients $\Gamma_\phi$ and $S_\phi$ of equation (13).

Solutions were obtained by using the FITS algorithm with uniform grids starting from 11 × 11 up to 81 × 81. *Figure 4* shows the grid dependence of the predictions for $Ra = 10^5$. The variation of the horizontal velocity component $U$ along the mid-vertical plane and the variation of $V$ and $\theta$ along the mid-height for different grids are shown in *Figure 4*. As shown in the figure, the results of 41 × 41 and 81 × 81 grids are virtually the same. *Table 4* depicts the CPU times and the values of $\Delta\tau$ for the sequence of grids used to obtain the final steady-state solution. The computational efficiency of FITS is calibrated against the FLOTRAN in *Table 4*, where the ratio of the CPU(min) on the VAX9000/420 computer between FITS and FLOTRAN is equal to 0.72.

To validate the present results, the FITS predictions at $Ra = 1.89 \times 10^5$ are compared with the experimental results of Krane and Jessee[11], the numerical results of Barakos *et al.*[12], and the results obtained from using the computer package FLOTRAN. The comparisons are shown in *Figure 5* for the variation of $U$ with $Y$ in the vertical midplane and the variation of 17 and 6 with $X$ in the horizontal midplane. These comparisons validate the results of the present algorithm. Moreover, as shown in the same figure the present variation of $U$ with $Y$ fits the experimental data of Krane and Jessee[11] slightly better than the results of Barakos and FLOTRAN.

In order to validate further the present results, the flow patterns and the isothermal contours at $Ra = 10^5$, $10^6$ and $10^8$ are compared with the corresponding contours of Barakos *et al.*[12] in *Figures 6, 7* and *8*. Moreover, the present contours of $Ra = 10^5$ are compared with the contours obtained by FLOTRAN in *Figure 6*. The comparisons show identical flow patterns. However, slight discrepancies appear in the isotherms among the solutions.

In *Table 5*, the present average Nusselt number ($\overline{Nu}$) is compared with other numerical solutions and data found in the literature at $Ra = 10^5$, $10^6$, and $10^8$. The average Nusselt number, $\overline{Nu}$ is defined as:

$$\overline{N_u} = \frac{\bar{h}H}{k} = -\int_0^1 \frac{\partial\theta}{\partial x}\, dY.$$

As shown in *Table 5*, the present values of $\overline{Nu}$ compare very well with the other predictions and data.

*Table 4* The present CPU time and time step $\Delta\tau$ for the sequence of the grids used with FITS and FLOTRAN (natural convection inside enclosure $Ra = 10^5$)

| Grid system | FITS 11 × 11 | FITS 21 × 21 | FITS 41 × 41 | FITS 81 × 81 | FLOTRAN 81 × 81 |
|---|---|---|---|---|---|
| CPU[a] (min) | 0.33 | 0.33 | 3.5 | 8.5 | 17.5 |
| $\Delta\tau$ | 0.14 | 0.11 | 0.09 | 0.06 | |

Note: VAX 9000/420 Super-mini (scalar mode)

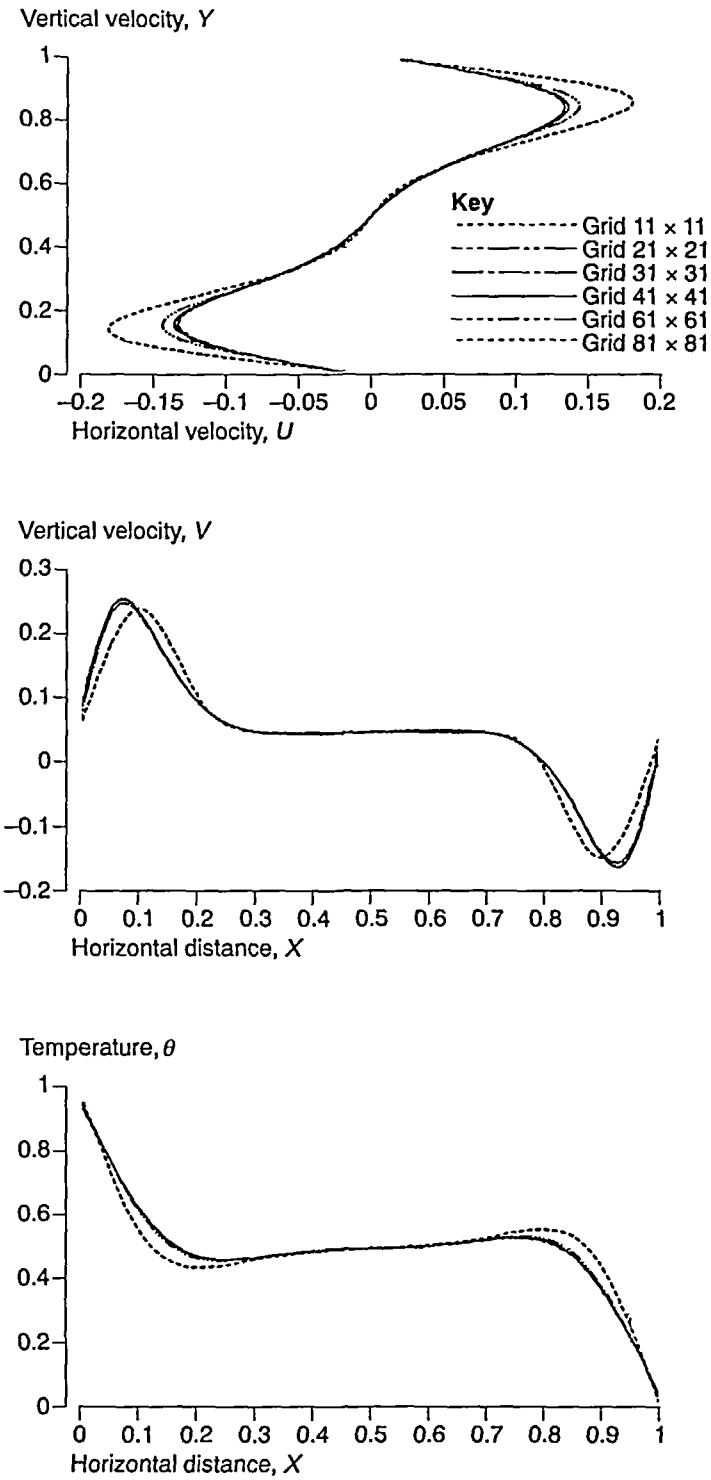


*Figure 4* Grid refinement tests for a thermal cavity with isothermal walls at $Ra = 10^5$

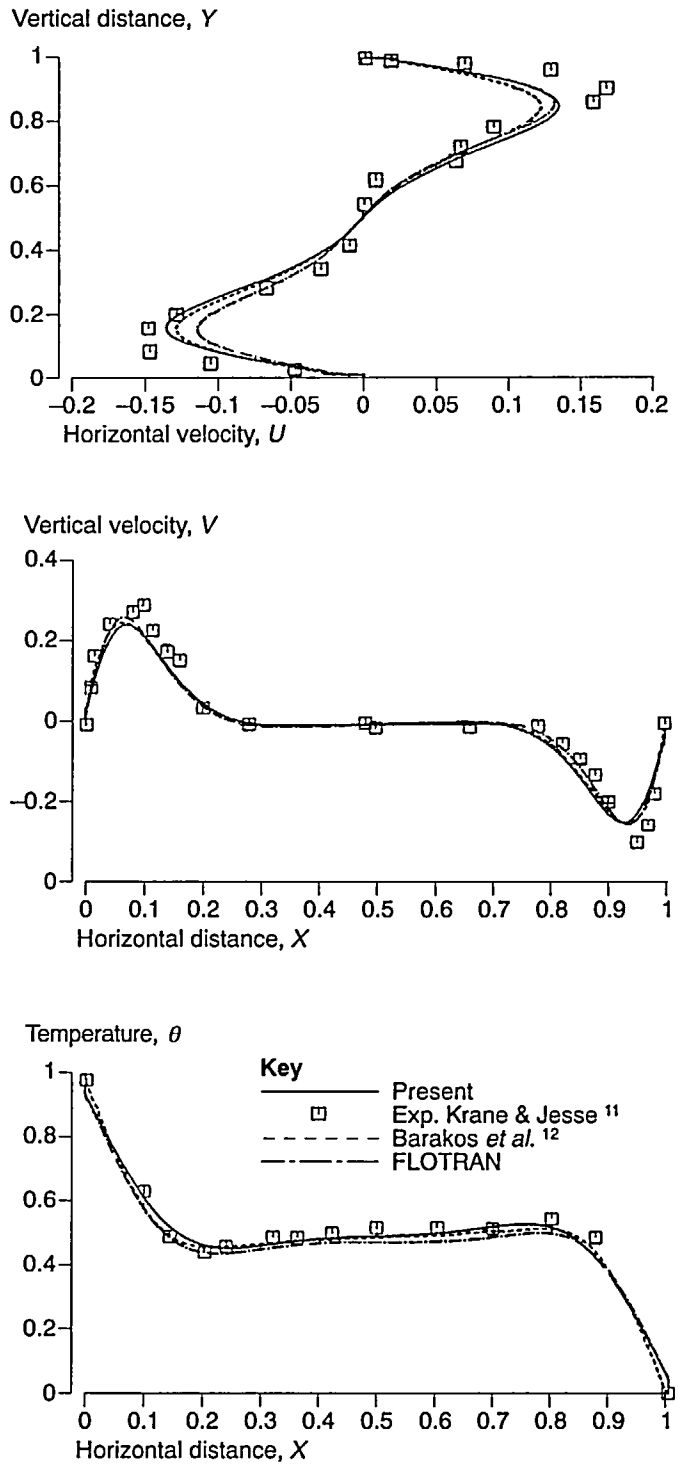


*Figure 5* Comparison of the present velocity and temperature profiles inside a thermal cavity with isothermal vertical walls ($Ra = 1.89 \times 10^5$) with other solutions and data

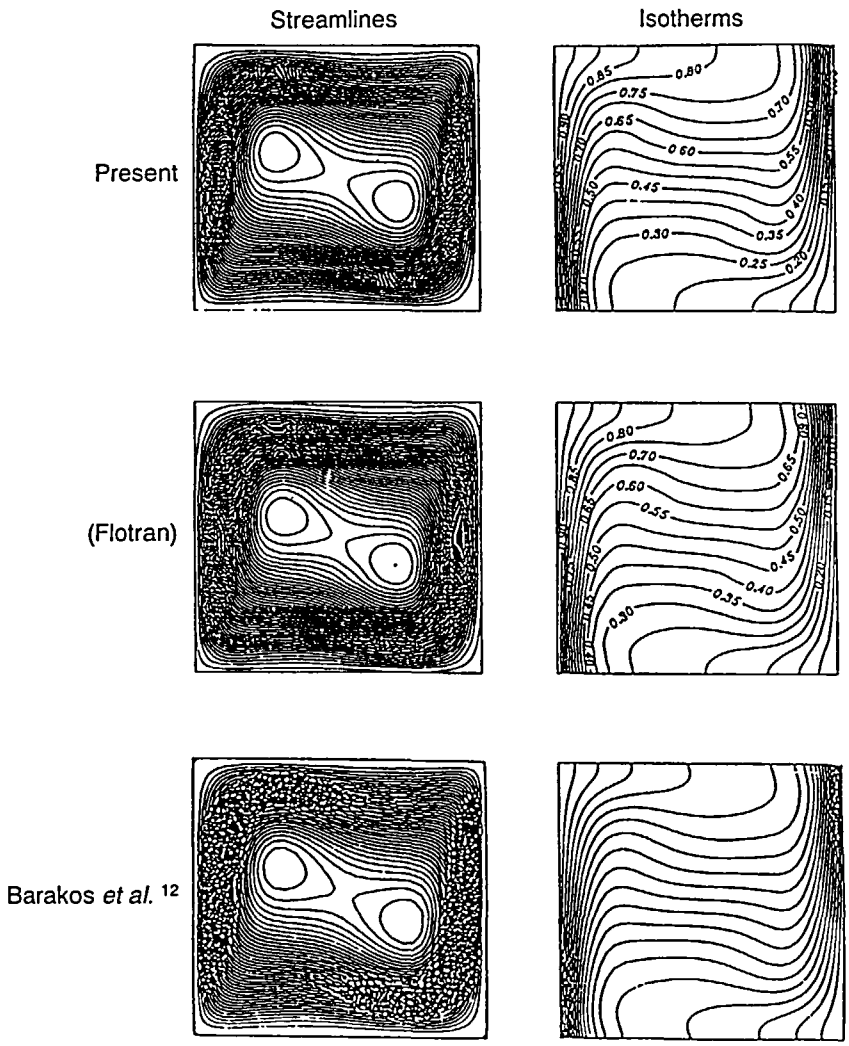


*Figure 6* Comparisons of the streamlines and isotherms inside a thermally driven vertical cavity between the present FITS predictions and other solutions at $Ra = 10^5$

*Table 5* Comparison of the present values of $\overline{Nu}$ calculated for thermal cavity with other solutions and data

| Work | Values of $\overline{Nu}$ $Ra = 10^5$ | $Ra = 10^6$ | $Ra = 10^8$ |
|---|---|---|---|
| Present work | 4.512 | 8.800 | 30.32 |
| Barakos *et al.*[12] | 4.510 | 8.806 | 30.10 |
| Markatos and Pericleous[13] | 4.430 | 8.754 | |
| De Vahl Davis and Jones[14] | 4.519 | 8.799 | |
| Fusegi *et al.*[15] | 4.646 | 9.012 | |
| Henkes *et al.*[16] | | | 30.4 |

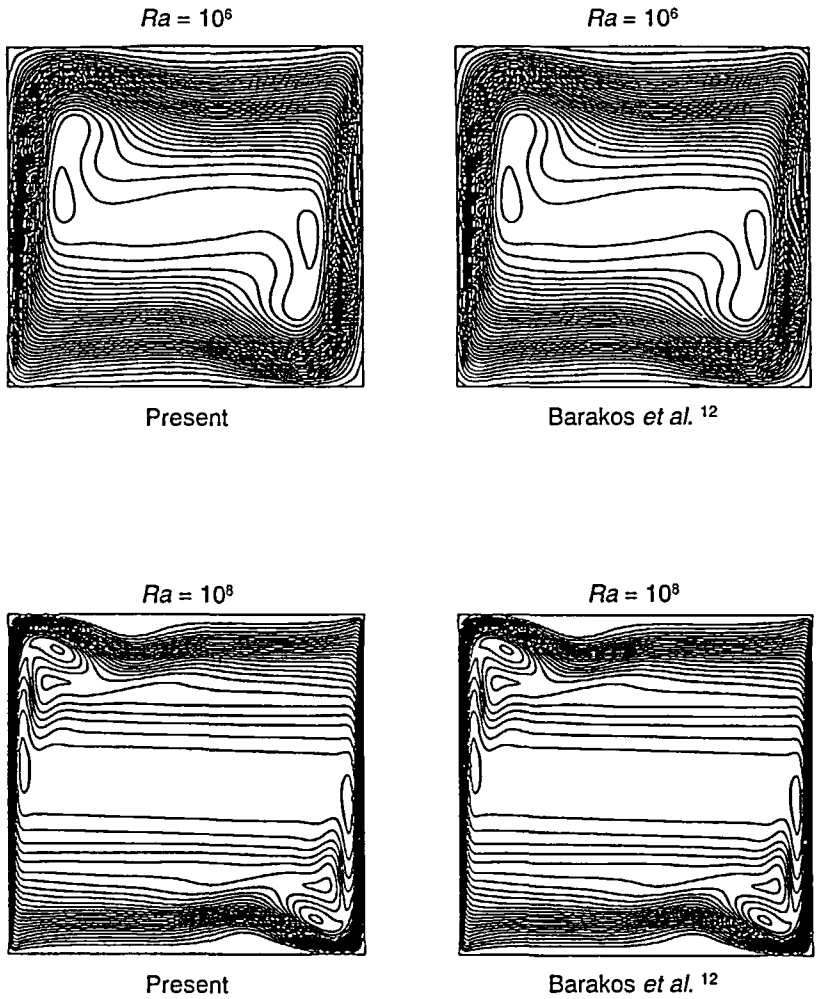


*Figure 7* Comparisons of streamlines inside a thermally driven cavity between the present FITS solution and the predictions of Barakos *et al.*[12] at $Ra = 10^6$ and $10^8$

## LAMINAR BUOYANCY-ASSISTED FLOW OVER A VERTICAL BACKWARD-FACING STEP

The third test problem represents the laminar buoyancy-assisted flow over a backward facing vertical step. This problem is commonly used as a benchmark test in computational fluids mechanics[17]. The flow of this problem experiences significant flow separation that depends mainly on the dimension of the step, the velocity at the inlet section as well as the temperature-difference between the two vertical walls.

The geometry of the present problem is shown in *Figure 9* together with the temperature and velocity boundary conditions at the walls. A fully developed parabolic channel flow profile was imposed at the inlet section where the vertical velocity component $V$ is given as:

$$V = \frac{3}{2}\left[1-(3-2X)^2\right], 1 < X < 2.$$

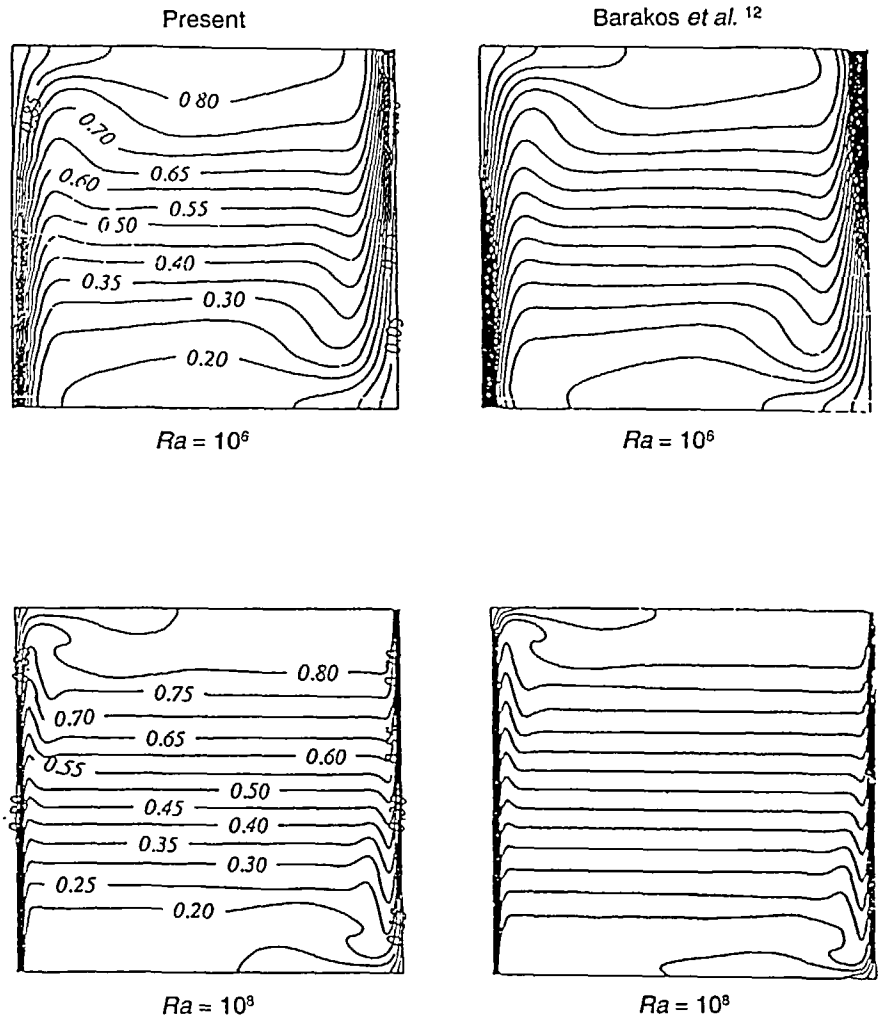


*Figure 8* Comparisons of isotherms inside a thermally driven cavity between the present FITS solutions and the predictions of Barakos *et al.*[12] at $Ra = 10^6$ and $10^8$

The length of the solution domain is 35 times the step height $S$. At the exit plane, the gradient of all variables in the $Y$-direction were set to zero. The vorticity transport equation and the energy equation are given by equations (19) and (13) with the coefficient $\Gamma_\Omega$, $S_\Omega$, $\Gamma_\theta$ and $S_\theta$ as given in *Table 1*. The reference parameters $H$, $u_{ref}$ and $\Delta T_{ref}$ for the present problem are also listed in *Table 1*.

Steady-state solutions have been computed using the present FITS procedure at $Re_s = 100$, $Pr = 0.7$ and for $Gr_s = 0$ and 1000. The computations were performed on a number of successive meshes ranging from coarse to fine grid sizes. The initial crude mesh $A$ is composed of uniform, but non-square, grids with 41 × 121 in the $X$ and $Y$ co-ordinates, respectively. The mesh was then successively refined as shown in *Table 6*. In the final refined mesh (meshes D & E) the grid size ($\Delta X$) was uniform in the $X$-direction with 91 and 101 respectively. In the $Y$-direction, the grid size $\Delta Y$ was also uniform in the region $-5 \leq Y \leq 7.5$ and then increased linearly in the region $7.5 \leq Y \leq 30$. The solutions were considered to be converged to steady-state when the maximum error-norm $\lambda$ (equation 26) was smaller than $10^{-6}$. A mesh independent solution was obtained with mesh $D$

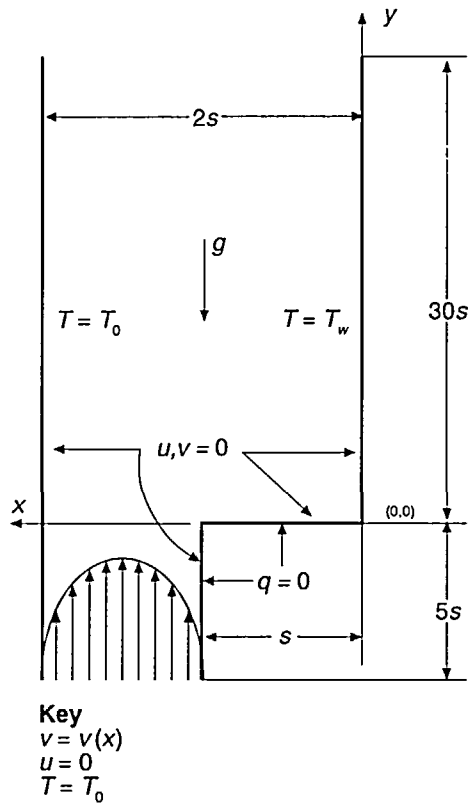


*Figure 9* Geometry and co-ordinates for a vertical buoyancy-assisted laminar backward-facing step flow

where the difference in the maximum velocity and temperature values were less than 1 per cent between meshes *D* and *E* for $Gr_s = 100$, $Pr = 0.7$ and $Re_s = 100$. *Table 6* shows the successive mesh characteristics and the computer (VAX9000/420) resources for $Gr_s = 1000$. The grid convergence behaviour of the reattachment lengths for the recirculation region at the hot wall $L_r$ is shown in *Table 7* for both the forced and mixed convection cases. Both the final (mesh *D*) reattachment lengths of the two cases compare very well with the previous numerical and experimental work presented in *Table 8*. The main reattachment point refers to the streamline from the step to the heated wall, *Figure 10*. The efficiency of the present FITS was calibrated against the SIMPLE finite volume method[21] for the mixed convection case ($Gr_s = 1000$). *Table 9* compares the total CPU times of both methods. It can be shown that the saving in CPU time between FITS and SIMPLE is about 41 per cent. In fact since the two solutions were performed on different models

*Table 6* Grid characteristics and computer CPU times for a vertstep flow with $Re_s = 100$, $Pr = 0.7$ and $Gr_s = 1000$.

| Mesh | Grids (M × N) | Dt | CPU(min)[a] |
|---|---|---|---|
| A – crude | 41 × 121 | 0.16 | 20.6 |
| B – medium 1 | 61 × 141 | 0.12 | 33.9 |
| C – medium 2 | 81 × 181 | 0.07 | 59.6 |
| D – fine 1 | 91 × 241 | 0.04 | 83.7 |
| E – fine 2 | 101 × 281 | 0.02 | 102.8 |

Note: [a]VAX 9000/420 Super-mini (scalar mode)

of the Digital Equipment Corporation VAX series, the actual CPU time of SIMPLE solution is approximately modified in the present work to account for the higher performance of the VAX9000/420 model relative to the VAX6530. The previous calibration confirms the high computational speed (convergence rate) of the present scheme.

To validate the present predictions, comparisons were carried out with the SIMPLE results of Cochran *et al.*[21], the finite difference results ofAcharya *et al.*[22], and the finite-element solution of Chopin[19]. *Figure 11* (which follows the Reference section) shows these comparisons for the variation of $U$, $V$ and $\theta$ with $X$ at $Y = 2$ and $G_{rs} = 10^3$. As shown in the figure the present predictions are in good comparison with the other solutions. Further comparisons to verify the present scheme are presented in *Figure 12* (which also follows the Reference section) the local Nusselt number and skin friction cofficient profiles, where:

$$Nu = -\frac{\partial \theta}{\partial X}$$

$$C_f Re_s = 2\frac{\partial U}{\partial X}$$

As shown the comparison is good.

*Table 7* Grid convergence behaviour of the reattachment lengths ($Lr$) for the recirculation region at the hot wall in vertical step flow

| Mesh | $Lr$ Forced flow $Gr_s = 0$ | $Lr$ Mixed flow $Gr_s = 1000$ |
|---|---|---|
| A – crude | 4.691 | 3.380 |
| B – medium 1 | 4.812 | 3.184 |
| C – medium 2 | 4.700 | 3.045 |
| D – fine 1 | 4.765 | 2.990 |

*Table 8* Reattachment lengths for recirculation region of step flow with $Re_s = 100$

| $Gr_s$ | Present | Lin *et al.*[18] | Chopin19 | Hong *et al.*[20] |
|---|---|---|---|---|
| 0 | 4.77 | 4.91 | 4.61 | 4.94 |

*Table 9* Comparison of the computer CPU time between the present predictions and the FV[SIMPLE] results of Cochran[21] for a vertical step flow with Res = 100, Pr = 0.7 and Grs = 1000

| Mesh | Present (FITS) Number of control volumes | CPU[a] (min) | FV(SIMPLE) of Cochran[21] Number of control volumes | CPU[b] (min) |
|---|---|---|---|---|
| A – crude | 4,961 | 20.6 | 1,080 | 22.3 |
| B – medium 1 | 8,601 | 33.9 | 3,600 | 84.3 |
| C – medium 2 | 14,661 | 59.6 | 7,200 | 229.1 |
| D – fine 1 | 21,931 | 83.7 | | |
| Total CPU (min) | | 197.8 | | 335.6 |

Notes:
[a]VAX9000/420 super-mini-computer (scalar mode)
[b]modified CPU time = CPU time on VAX6530 × {*speed of VAX6530/speed of VAX9000(420)*}

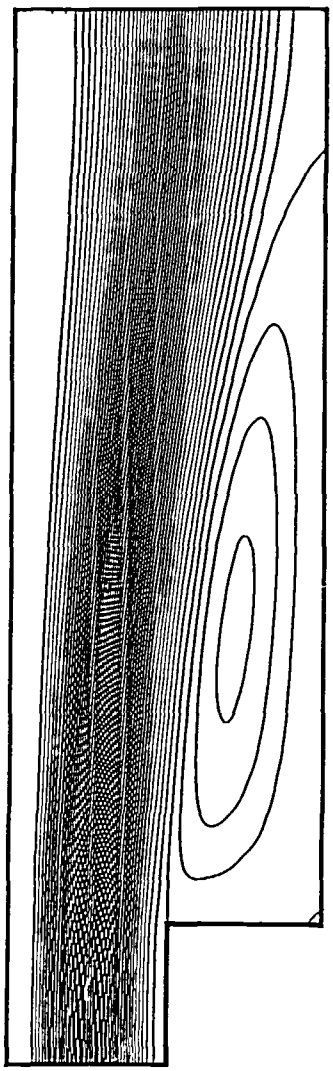

*Figure 10* Streamlines for a step flow at $Re_s = 100$ and $Gr = 0$

## CONCLUSION

The solutions of the three benchmark problems reveal that the FITS algorithm is efficient and accurate in solving different buoyancy-assisted internal steady flows. Based on the present predictions, it can be concluded that the weak stability restriction on the time step FITS is considerably relieved by the use of FITS algorithm. This advantage permits the use of a larger time increment and hence results in a significant increase of the convergence rate towards steady-state.

A further extension to be investigated is the application of the algorithm to the modelling of turbulent flows. This work is progressing and will be reported later this year.

## REFERENCES


1 Ghia, K.N. and Ghia, U., Elliptic systems: finite difference method III, in Minkowycz, W.J., Sparrow, E.M., Schneider, G.E. and Pletcher, R.H. (Eds), *Handbook of Numerical Heat Transfer*, John Wiley & Sons, Inc., New York (1988)

2 McDonough, M W. and Faghri, A., Experimental and numerical analysis of the natural convection for water through its density maximum in a rectangular enclosure, *Int. J. Heat Mass Transfer*, **37**, 783-801 (1994)

3 Patankar, S.V., *Numerical Heat and Fluid Flow*, Hemisphere, New York (1980)

4 Pletcher, R.H., Minkowycz, W.J., Sparrow, E.M. and Schneider, G.E., Overview of basic numerical methods, in Minkowycz, W.J. *et al.* (Eds), *Handbook of Numerical Heat Transfer*, John Wiley & Sons, Inc., New York (1988)

5 Richtmyer, R.D., and Morton, K.W., *Difference Methods for Initial-value Problems*, 2nd edition, Interscience Publishers, J. Wiley & Sons, New York (1967)

6 Versteeg, H.K. and Malalasekera, W., *An Introduction to Computational Fluid Dynamics (The Finite Volume Method)*, Longman Scientific & Technical, Longman Group Ltd, Harlow (1995)

7 Abbot, M.B. and Basco, D.R., *Computational Fluid Dynamics*, Longman Scientific and Technical, London (1990)

8 Hoffman, K. and Chiang, S., *Computational Fluid Dynamics for Engineers*, Vol. I, Engineering Education System, Wichte, KS 67208-1078, USA (1993)

9 Churbanov, A.G., Vabishchevich, P.N., Chudanov, V.V. and Strizhov, V.F., A numerical study on natural convection of heat-generating fluid in rectangular enclosures, *Int. J. Heat and Mass Transfer*, **37**, 18, 2969-2984 (1994)

10 Ostrach, S., Natural convection in enclosures, *Trans. ASME, J. Heat Transfer*, **110**, 1175-1190 (1988)

11 Krane, R.J. and Jessee, J., Some detailed field measurements for a natural convection flow in a vertical square enclosure, *Proc. 1st ASME-JSHE Thermal Engineering Joint Conf.*, **1**, 323-329 (1983)

12 Barakos, G., Mitsoulis, E. and Assimacopoulos, D., Natural convection flow in a square cavity revisited: laminar and turbulent models with wall functions, *Int. J. for Numerical Methods in Fluids*, **18**, 695-719 (1994)

13 Markatos, N.C. and Pericleous, K.C., Laminar and turbulent natural convection in an enclosed cavity, *Int. J. Heat Mass Transfer*, **27**, 772-775 (1984)

14 De Vahl Davis, G. and Jones, I.P., Natural convection of air in a square cavity: a comparison exercise, *Int. J. Numer. Methods Fluids*, **3**, 227-248 (1983)

15 Fusegi, T., Hyun, J.M., Kuwahara, K. and Farouk, B., A numerical study of three-dimensional natural convection in a differentially heated cubical enclosure, *Int. J. Heat Mass Transfer*, **34**, 1543-1557 (1991)

16 Henkes, R.A.W., van der Vlugt, F.F. and Hoogendoorn, C.J., Natural convection flow in a square cavity calculated with low-Reynolds-number turbulence model, *Int. J. Heat Mass Transfer*, **34**, 1543-1557 (1991)

17 Blackwell, B.F. and Armaly, B.F. (Eds), *Computational Aspects of Heat Transfer – Benchmark Problems*, ASME HTD, **258** (1993)

18 Lin, J.T., Armaly, B.F. and Chen, T.S., Mixed convection in buoyancy-assisted vertical backward-facing step flows, *Int. J. Heat Mass Transfer*, **33**, 10, 2121-2132 (1990)

19 Chopin, T.R., Mixed convection flow and heat transfer in a vertical backward facing step using the FLOTRAN CFD Program, in Blackwell, B.F. and Armally, B.F. (Eds), *Computational Aspects of Heat Transfer-Benchmark Problems*, ASME HTD, **258** (1993)

20 Hong, B., Armaly, B.F. and Chen, T.S , Mixed convection in a laminar, vertical, backward-facing step flow, in Blackwell, B.F. and Armaly, B.F. (Eds), *Computational Aspects of Heat Transfer-Benchmark Problems*, ASME HTD, **258** (1993)

21 Cochran, R.J., Horstman, R.H., Sun, Y.S. and Emery, A.F., Benchmark solution for a vertical, buoyancy-assisted laminar backward-facing step flow using finite element, finite volume, and finite difference methods, in Blackwell, B.F. and Armaly, B.F. (Eds), *Computational Aspects of Heat Transfer-Benchmark Problems*, ASME HTD, **258** (1993)

22 Acharya, S., Dixit, G. and Hou, Q., Laminar mixed convection in a vertical channel with a backstep: a benchmark study, in Blackwell, B.F. and Armaly, B.F. (Eds), *Computational Aspects of Heat Transfer-Benchmark Problems*, ASME HTD, **258** (1993)

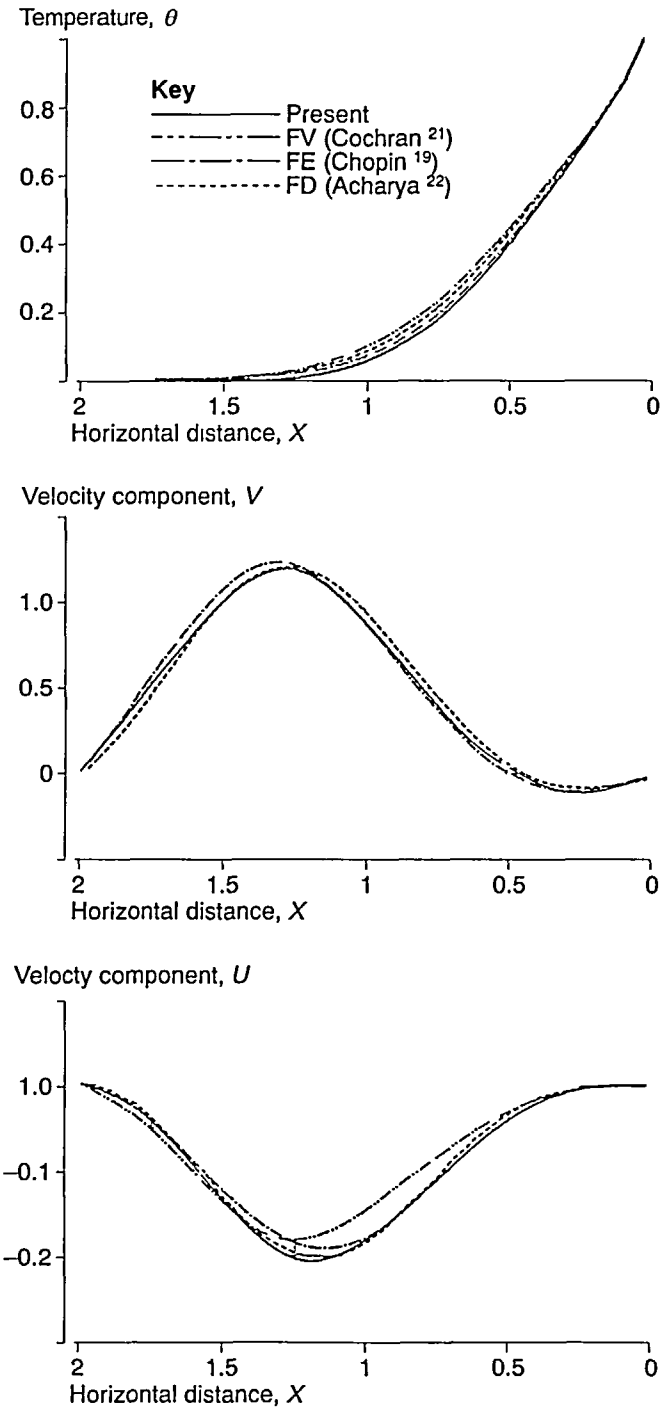


*Figure 11* Velocity components and temperature profiles along the horizontal axis $X$ for a step flow at $Y = 2$, $Re_s = 10^2$ and $Gr_s = 10^3$

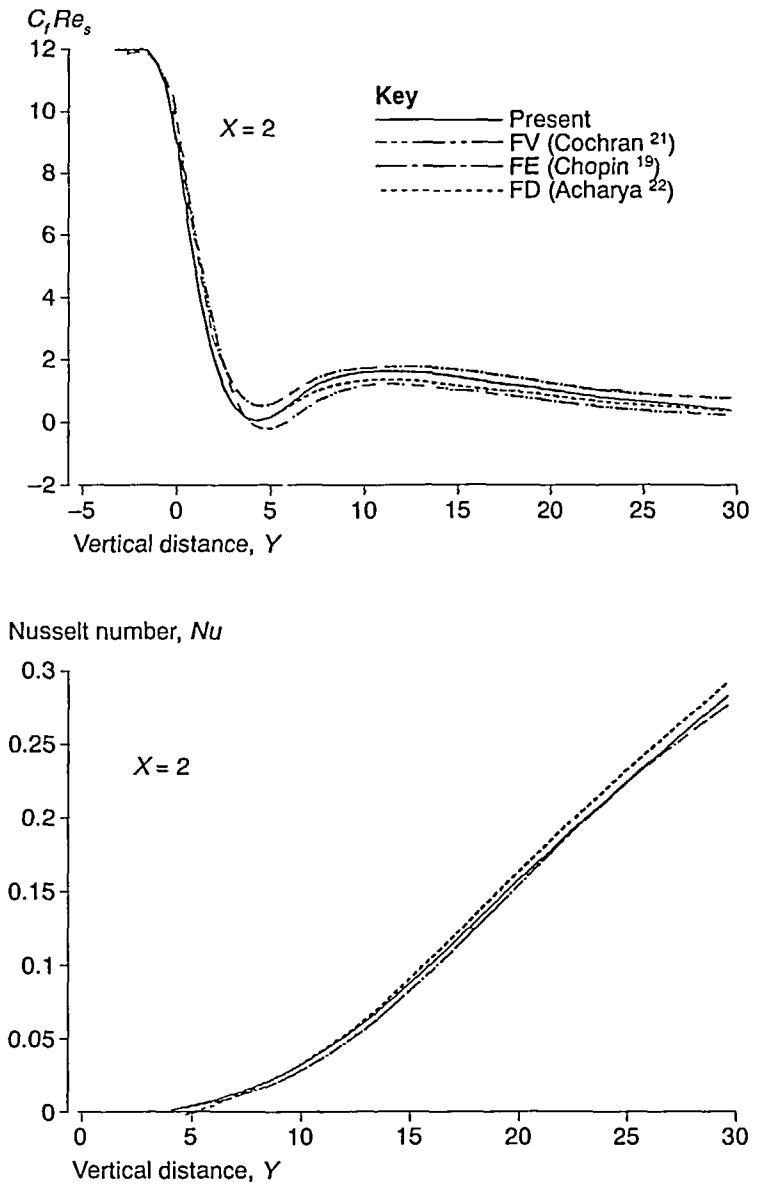


*Figure 12* Variations of the skin friction $C_f Re_s$ and the Nusselt number $Nu$ along the cold vertical wall at $Re_s = 10^2$ and $Gr_s = 10^3$